Structure of the neutron-rich nucleus ^{30}Mg

H. Nishibata,[1,*] K. Tajiri,[1,†] T. Shimoda,[1] A. Odahara,[1] S. Morimoto,[1] S. Kanaya,[1] A. Yagi,[1] H. Kanaoka,[1] M. R. Pearson,[2] C. D. P. Levy,[2] M. Kimura,[3] N. Tsunoda,[4] and T. Otsuka[5,6,7]

[1]*Department of Physics, Osaka University, Osaka 560-0043, Japan*
[2]*TRIUMF, 4004 Wesbrook Mall, Vancouver, British Columbia V6T 2A3, Canada*
[3]*Department of Physics, Hokkaido University, Sapporo 060-0810, Japan*
[4]*Center for Nuclear Study, the University of Tokyo, Tokyo 113-0033, Japan*
[5]*RIKEN, Saitama 351-0198, Japan*
[6]*National Superconducting Cyclotron Laboratory, Michigan State University, East Lansing, Michigan 48824, USA*
[7]*Instituut voor Kern-en Stralingsfysica, Katholieke Universiteit Leuven, B-3001 Leuven, Belgium*

(Received 25 June 2020; accepted 16 October 2020; published 25 November 2020)

Structure of the neutron-rich nucleus ^{30}Mg, which is located close to the region of the $N = 20$ "island of inversion," has been investigated by β-γ spectroscopy of spin-polarized ^{30}Na. From the detailed γ-γ coincidence relations, nine new states have been established in ^{30}Mg. The spin-polarization of ^{30}Na enabled firm spin-parity assignments for seven states in ^{30}Mg by means of the spatial asymmetry of β-ray counts in coincidence with the ^{30}Mg γ rays. Based on the experimental information, it is shown that various characteristic structures coexist in ^{30}Mg: (i) the ground-state vibrational-like band, (ii) the deformed band built on the 0^+_2 state at 1.788 MeV, (iii) the γ-vibrational band built on the 2^+_3 state at 3.543 MeV, and (iv) four states around 5 MeV associated with large β-transition probabilities: 1^+ and 2^+ states with spherical nature, 1^+ and 2^+ states with collective nature. The experimental results are compared with three theoretical calculations of the CHFB + LQRPA, the AMD + GCM, and the large-scale shell model with the EEdf1 interaction. All these theories reasonably reproduce the three bands.

DOI: 10.1103/PhysRevC.102.054327

I. INTRODUCTION

The neutron-rich nucleus ^{30}Mg ($Z = 12$, $N = 18$, $T_{1/2} =$ 335(17) ms [1]) has been attracting much attention since its discovery as a bound nucleus [2]. For the neutron-rich nuclei, which are located in the nuclear chart close to the $N = 20$ neutron magic number nucleus ^{32}Mg, the anomalous binding energies were noticed [3,4]. Later, their structures were found to differ from what were expected from the neutron magic number [5]. The region in the nuclear chart around ^{32}Mg was symbolically named the "island of inversion" [6].

The ISOL-based radioactive beam facility, the CERN Isotope mass Separator On-Line facility (ISOLDE), has enabled β-decay studies of these neutron-rich nuclei [7]. The excited states in ^{30}Mg have been investigated by the β decay of ^{30}Na [8–12], the β-delayed one-neutron (βn) decay of ^{31}Na [11,13], and the β-delayed two-neutron ($\beta 2n$) decay of ^{32}Na [13,14]. One of the important results was the spin-parity assignment for the second 0^+ state at 1.788 MeV [11,12]. The small $E0$ transition strength $\rho^2(E0,\ 0^+_2 \rightarrow 0^+_1)$, which was determined from the conversion electron measurement, indicated a large deformation of the 0^+_2 state [12]. Contrarily, the 0^+_1 ground state has been thought spherical [15], since it was described well by the shell-model calculation with a model space limited in the *sd* shell [16]. In this way, the picture that the spherical 0^+_1 ground state and the deformed 0^+_2 state at 1.788 MeV coexist in ^{30}Mg has been adopted.

The relation of the two 0^+ states is in sharp contrast with that in ^{32}Mg, which has 2 more neutrons than ^{30}Mg: the deformed 0^+_1 ground state and the spherical 0^+_2 state at 1.058 MeV coexist in ^{32}Mg [7]. These phenomena show the effects of the shell evolution [17].

The theoretical studies on the ^{30}Mg structure have shown much progress. The large-amplitude collective dynamics theory (CHFB + LQRPA) [18] predicted three bands in ^{30}Mg: the spherical ground-state band (0^+_1, 2^+_1, 4^+_1, 6^+_1), the deformed rotational band (0^+_2, 2^+_2, 4^+_2, 6^+_2), and the γ-vibrational band (2^+_3, 3^+_1, 4^+_3, 5^+_1, 6^+_3) [19]. Note that, for ^{32}Mg this theory raised a question on the naive picture of the deformed 0^+ ground and the spherical 0^+ excited states by showing large-amplitude quadrupole-shaped fluctuations in these states [19]. The recent large-scale shell-model calculation with the EEdf1 interaction showed significant configuration mixing in both the ground-state and the deformed bands [20].

The experimental knowledge on the excited levels in ^{30}Mg is still limited, even after almost 50 years of discovery. As discussed in the next section (II), the established spins and parities are only for the lowest three levels of 0^+_1, 2^+_1,

*Present address: Department of Physics, Kyushu University, Fukuoka 819-0395, Japan; nishibata@phys.kyushu-u.ac.jp
†Present address: Mitsubishi Electric Corporation, Hyogo 661–8661, Japan.

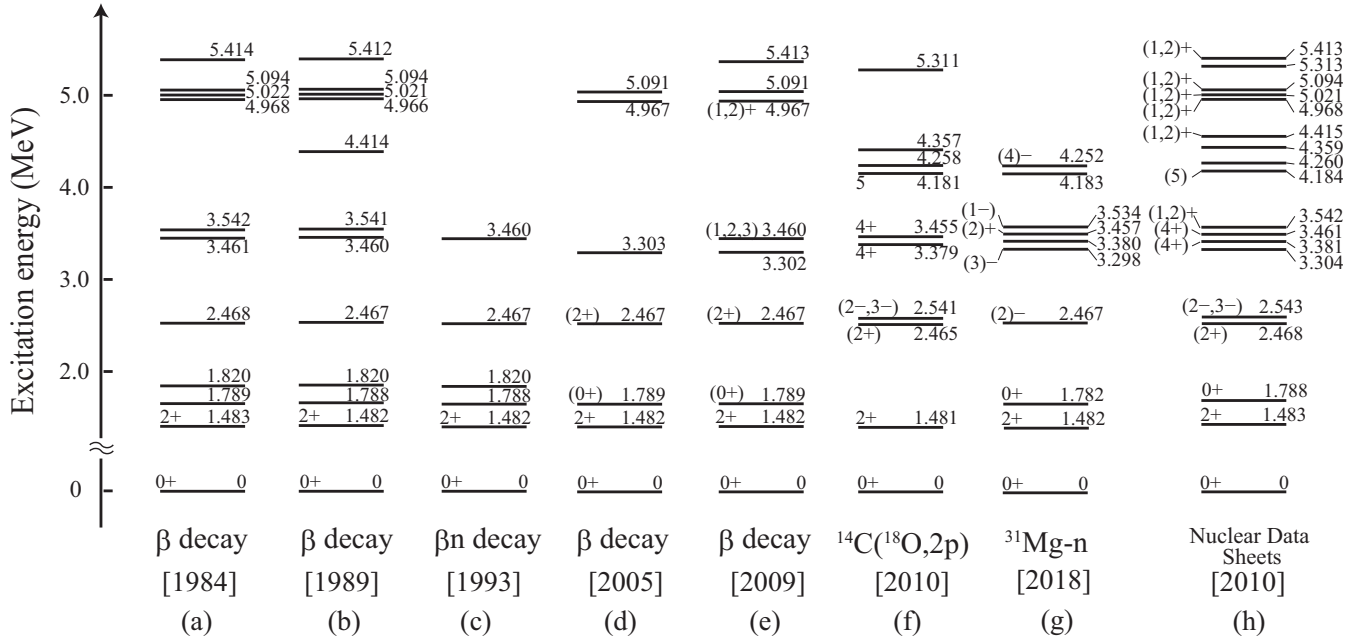

FIG. 1. Experimental levels in ^{30}Mg, established in the β-decay of ^{30}Na [(a) Ref. [9], (b) Ref. [10], (d) Ref. [11], and (e) Ref. [12]], βn decay [(c) Ref. [13]], the fusion-evaporation reaction of ^{14}C(^{18}O, p) [(f) Ref. [21]], and the intermediate energy one-neutron removal reaction of ^{31}Mg [(g) Ref. [20]]. The adopted levels in the evaluated data compilation (Nuclear Data Sheets) are also shown in (h) Ref. [1].

and 0_2^+, among 18 known levels in ^{30}Mg [1]. It is clear that the spin-parity assignment is essential to compare the experimental data with the theoretical predictions on the level-by-level basis.

To firmly assign the spins and parities and thereby to clarify the nuclear structure of ^{30}Mg, we have performed an experiment by β-γ spectroscopy of spin-polarized ^{30}Na($I^{\pi}_{\text{g.s.}} = 2^+$, $T_{1/2} = 48(2)$ ms [1], $Q_\beta = 17.358(6)$ MeV [22]) at the new generation ISOL-based radioactive Isotope Separation and Acceleration (ISAC) facility at TRIUMF. The effectiveness of the use of polarization has been discussed in our papers on the experimental evidence for the shape coexistence in ^{31}Mg [23,24].

II. HISTORICAL REVIEW OF LEVEL STRUCTURE OF ^{30}Mg

The level structure of ^{30}Mg has been studied by various types of experiments: the β decay of ^{30}Na [8–12], the βn decay of ^{31}Na [11,13], the $\beta 2n$ decay of ^{32}Na [13,14], the fusion-evaporation reaction of ^{14}C(^{18}O, $2p$) [21], and the one-neutron removal reaction of ^{31}Mg [20]. Figure 1 summarizes the experimental level schemes in historical order, together with the evaluated and adopted levels in the Nuclear Data Sheets [1].

The excited levels at 1.484[1] and 2.470 MeV in ^{30}Mg were observed for the first time in the β decay of ^{30}Na at ISOLDE [8]. They reasonably proposed the 2_1^+ spin-parity assignment for the 1.484-MeV level because of the most abundant γ-ray peak. In their successive experiment [9], they proposed 10 excited levels at 1.483, 1.789, 1.820, 2.468, 3.461, 3.542, 4.968, 5.022, 5.094, and 5.414 MeV. Another group's β-decay experiment added a new level at 4.414 MeV [10]. In the βn decay of ^{31}Na [13], the levels at 1.482, 1.788, 1.820, 2.467, and 3.460 MeV were confirmed. Up to then, no spin-parity assignment has been done, except for the 2_1^+ level.

The Coulomb excitation experiment provided us with new information of the reduced transition probability as $B(E2; 0^+ \rightarrow 2^+) = 295(26)\ e^2\ \text{fm}^4$ [15]. This value was consistent with that predicted by the shell-model calculation assuming a spherical 0p0h configuration [16]. Thus, the spherical ground-state picture has been adopted for ^{30}Mg. The later Coulomb excitation experiment at lower beam energy reported a somewhat smaller value of 241(31) e^2 fm^4 [25].

In another β-decay experiment by the group of Ref. [11], they examined the γ-γ coincidence relation, and they found that the 1789-keV[2] γ ray originates from the decay from the 5.091-MeV level to a new level at 3.303 MeV and the 1820-keV γ ray is due to the decay of 3.303 $\rightarrow$ 1.482. As a result, they proposed to add a new level at 3.303 MeV and to remove the 1.820-MeV level from the ^{30}Mg level scheme. They also observed a long half-life [$T_{1/2} = 3.9(4)$ ns] of the 1.789-MeV level. Based on the suggested $E2$ nature of the 306-keV transition (1.789 $\rightarrow$ 1.482), they proposed the (0_2^+) assignment[3] for the 1.789-MeV level. For the 2.467-MeV level, they also proposed (2^+) assignment, because of the dominant $M1$ nature of the 985-keV γ transition (2.467 $\rightarrow$ 1.482).

[1]Hereinafter, the energies of the level and γ rays are quoted from the original paper.

[2]Hereinafter, the γ-ray energies are shown in units of keV.

[3]The parentheses are given for tentative assignments.

The 0_2^+ assignment for the 1.789-MeV level was confirmed by the conversion electron measurement [12]. As mentioned before, they identified the $E0$ transition (1.789 MeV $\rightarrow$ g.s.) and found the small transition strength between the 0_1^+ and 0_2^+ levels, as mentioned before. This fact indicates a large deformation of the 0_2^+ level [12]. Since then, the deformed 0_2^+ state picture has been adopted.

A highly sensitive measurement for the fusion reaction of ^{14}C(^{18}O, $2p$) at 37 MeV revealed the higher spin levels up to $I = 5$ [21]. From the γ-ray angular distribution analysis, they proposed a 4^+ assignment for a new level at 3.379 MeV.

In a recent intermediate energy one-neutron removal reaction from ^{31}Mg, the longitudinal momentum distribution of ^{30}Mg was measured in coincidence with γ rays [20]. They obtained a smaller spectroscopic factor for the 0_2^+ level than that expected from the picture that the 0_2^+ level is dominated by the 2p2h configuration. Note that they proposed a negative-parity assignment of $(2)^-$ for the 2.467-MeV level, for which the (2^+) assignment is adopted [1].

III. EXPERIMENT

The experiment was performed at the ISAC facility of TRIUMF [26] in the same beam time as the experiment with the ^{31}Na beam [23,24]. The principle of spin-parity assignment and the experimental setup were exactly the same as those in the ^{31}Na-beam experiment. The details are found in Ref. [24].

The nuclear-spin-polarized radioactive beam of ^{30}Na with an energy of 28 keV was produced by a target fragmentation reaction with a 500-MeV 10-μA proton beam on a UC$_x$ target. The spin-polarized ^{30}Na beam was produced by the collinear optical pumping at the polarizer [27] and was delivered to the experimental setup for the β-γ spectroscopy. The ^{30}Na beam intensity was 2.4×10^3 particles per second after the polarizer. The polarization of ^{30}Na was 31(1)%, as will be discussed in Sec. IV B 2.

Figure 2 shows the experimental setup. The transversely spin-polarized ^{30}Na beam came from the lower left side of the figure and was stopped in vacuum on a 20-μm-thick Pt foil. To preserve the polarization, a static magnetic field of 0.53 T was applied to the Pt foil along the polarization direction. The β rays and the β-delayed γ rays after the β decay of ^{30}Na were distinguishably detected by eight sets of detector telescopes consisting of a coaxial high-purity Ge detector (HPGe) and thin plastic scintillator(s) in front of the HPGe. As shown in Fig. 2, two of the telescopes were placed along the polarization direction close to the Pt foil so as to measure the spatial asymmetry of β-ray counts in coincidence with the ^{30}Mg γ rays. Six other telescopes were placed in a plane perpendicular to the polarization direction.

The β-ray angular distribution in the allowed transitions is expressed as $W(\theta) \sim 1 + AP\cos\theta$, with the asymmetry parameter A of the β transition, the ^{30}Na polarization P, and the β-ray emission angle θ with respect to the polarization direction. Therefore, the 0°–180° asymmetry of β-ray counts determines the AP value for each transition. Note that the asymmetry parameter A strongly depends on the daughter-state spin. From the experimental A value, the spin value of the ^{30}Mg state is determined. Parities of the ^{30}Mg states populated by the allowed transition should be positive, since the parity of ^{30}Na$_{\text{g.s.}}$ is positive.

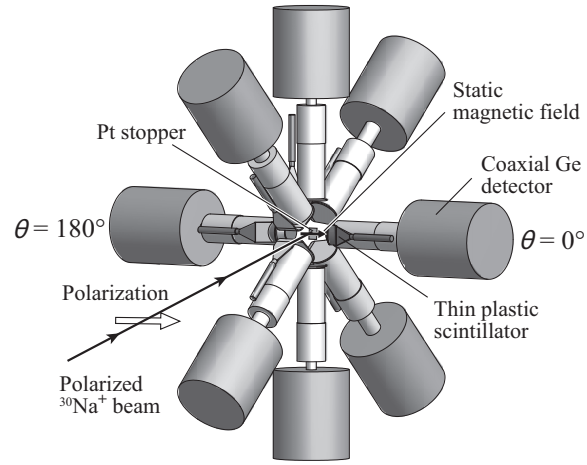

FIG. 2. Experimental setup. The ^{30}Na$^+$ ion beam with spin polarization in the direction shown by a thick open arrow was delivered in vacuum from the lower left-side and was stopped in the Pt stopper foil. The β rays and γ rays in the decay of ^{30}Na were detected by eight detector telescopes, each consisting of front thin plastic scintillator(s) and a back Ge detector. Two telescopes labeled "$\theta = 0°$" and "$\theta = 180°$" measured the β-decay asymmetry.

The preliminary results in our previous experiment have been reported elsewhere [28]. Thanks to the UC$_x$ target development, the much higher intensity beam enabled higher statistics measurement even with a short beam time (6.7 hr) in the present work. Most of the previously reported results were confirmed, but some have been revised.

IV. EXPERIMENTAL RESULTS

A. Decay scheme of ^{30}Na $\xrightarrow{\beta}$ ^{30}Mg

1. Absolute β- and γ-transition intensities

To establish the decay scheme of ^{30}Na $\xrightarrow{\beta}$ ^{30}Mg, the absolute intensities of β and γ rays should be evaluated. Those were obtained in a similar way to that described in Ref. [24].

In the first step, we need the numbers of the implanted nuclei $N(^{30}\text{Na})$, the β-decay daughter nuclei $N(^{30}\text{Mg})$, the βn-decay daughter nuclei $N(^{29}\text{Mg})$, and the $\beta 2n$-decay daughter nuclei $N(^{28}\text{Mg})$. The numbers of nuclei $N(^{30}\text{Mg})$ and $N(^{29}\text{Mg})$ were estimated from the 444-keV γ-ray counts in ^{30}Al (daughter of ^{30}Mg) and the 2224-keV γ-ray counts in ^{29}Al (daughter of ^{29}Mg), respectively: $N(^{30}\text{Mg}) = N_{\gamma 444}/(\varepsilon_{\gamma 444} I_{\gamma 444})$ and $N(^{29}\text{Mg}) = N_{\gamma 2224}/(\varepsilon_{\gamma 2224} I_{\gamma 2224})$, with the number of γ-ray counts $N_{\gamma E_\gamma}$, the γ-ray detection efficiency $\varepsilon_{\gamma E_\gamma}$, and the absolute intensity of the γ transition with an energy of E_γ, $I_{\gamma E_\gamma}$, per respective parent nucleus decay. The absolute intensities of $I_{\gamma 444}$ in ^{30}Al [29] and $I_{\gamma 2224}$ in ^{29}Al [9] are well established. However, it was not possible to estimate the number of ^{28}Mg nuclei $N(^{28}\text{Mg})$ from its daughter γ rays because of the long half-life of ^{28}Mg (20.9 h). Therefore, we adopted the reported value of the $\beta 2n$-branching ratio $P_{2n} = 1.15(25)\%$ per ^{30}Na decay [9].

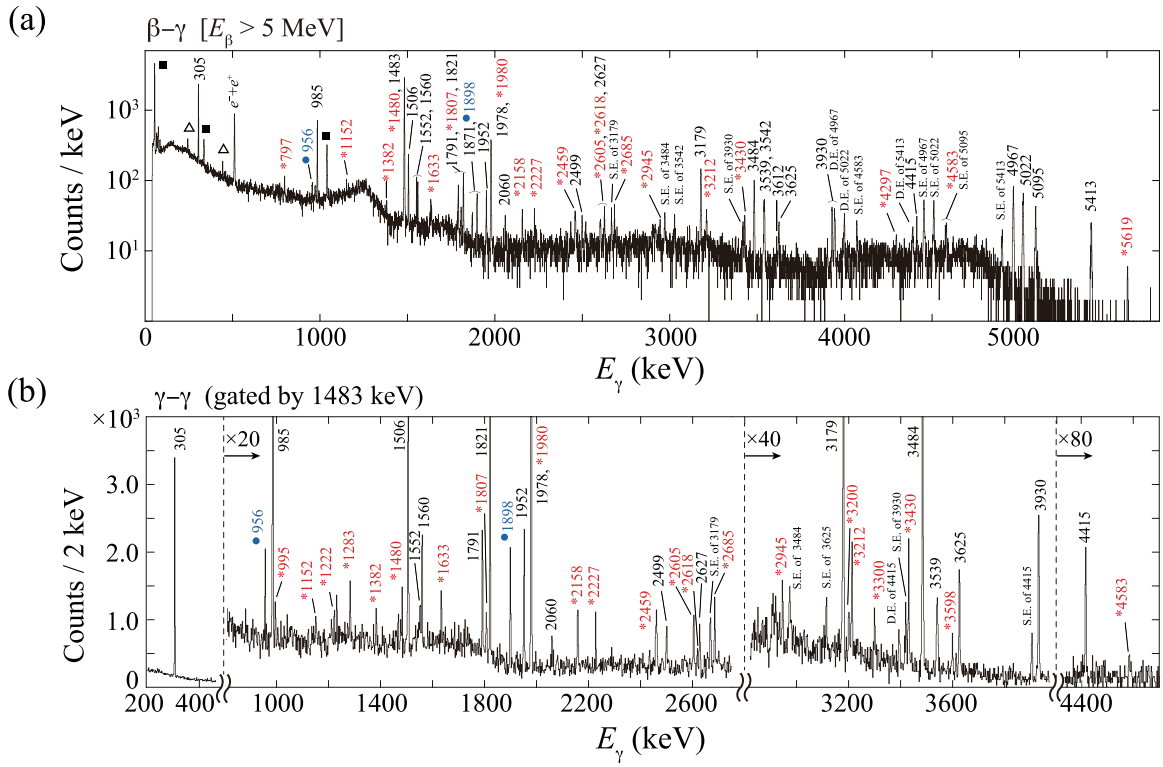

FIG. 3. (a) Gamma-ray energy spectrum in coincidence with β rays ($E_\beta > 5$ MeV), and (b) γ-ray coincidence spectrum gated by the 1483-keV γ ray. The γ-ray peaks with energy in units of keV are the γ rays in ^{30}Mg. The peaks labeled with $*$ (shown in red) are newly observed γ rays. The peaks labeled with • (blue) are due to the known γ-ray transitions in ^{30}Mg, but newly observed in the β decay of ^{30}Na. The peaks labeled with ■ and △ are due to the βn decay of ^{30}Na and the β decay of ^{30}Mg, respectively.

In the second step, the number of ^{30}Na nuclei $N(^{30}\mathrm{Na})$ was estimated from the relation $N(^{30}\mathrm{Na}) = [N(^{30}\mathrm{Mg}) + N(^{29}\mathrm{Mg})]/(1 - P_{2n})$. Then, the absolute intensity of the 1483-keV γ ray in $^{30}\mathrm{Mg}(2_1^+ \to 0_1^+)$ was estimated as $I_{\gamma 1483} = 39(4)\%$ per ^{30}Na decay, from the relation $I_{\gamma 1483} = N_{\gamma 1483}/[\varepsilon_{\gamma 1483} \mathrm{N}(^{30}\mathrm{Na})]$. The βn-branching ratio P_n was estimated from the relation of $P_n = (1 - P_{2n})N(^{29}\mathrm{Mg})/[N(^{30}\mathrm{Mg}) + N(^{29}\mathrm{Mg})]$ as $P_n = 33(5)\%$.

These values are consistent with those adopted in the Nuclear Data Sheets [1], $I_{\gamma 1483} = 44(3)\%$ and $P_n = 30(4)\%$. We evaluated the absolute γ- and β-transition intensities based on our $I_{\gamma 1483}$ and P_n values.

The absolute γ-transition intensities I_γ in ^{30}Mg were obtained by referring to the $I_{\gamma 1483}$ value. The absolute β-transition intensities I_β in $^{30}\mathrm{Na} \xrightarrow{\beta} {}^{30}\mathrm{Mg}$ were obtained from the imbalance between populating and depopulating γ-transition intensities for each level.

2. *Newly observed γ rays in* ^{30}Mg *and revised decay scheme of* $^{30}\mathrm{Na} \xrightarrow{\beta} {}^{30}\mathrm{Mg}$

Figure 3(a) shows the γ-ray energy spectrum in coincidence with β rays. Only for this figure, the β-ray-energy[4] gate of $E_\beta > 5$ MeV was set to reduce the background γ rays from the activities in the ^{30}Na decay chains of β, βn, and $\beta 2n$. Figure 3(b) shows the γ-ray coincidence spectrum gated by the 1483-keV γ ray ($2_1^+ \to 0_1^+$) in ^{30}Mg, with a time window of ±800 ns.

The γ-ray peaks with the energy in keV are due to transitions in ^{30}Mg. The peaks labeled with $*$ (shown in red) are newly observed γ rays. The peaks labeled with • (blue) are due to the known γ-ray transitions in ^{30}Mg, but newly observed in the β decay of ^{30}Na. The peaks labeled with ■ and △ are due to the βn decay of ^{30}Na and the β decay of ^{30}Mg, respectively.

Table I shows the coincidence relations with the 1483-keV γ ray. From similar examinations of the γ-γ coincidence relations between all 55 γ rays, we have successfully assigned these γ rays as due to the deexcitation in ^{30}Mg. Note that the β-decay experiments in the past have assigned 27 γ rays in ^{30}Mg [1], thus we could double the number of assigned γ rays in the present work.

From the coincidence relations and energy consistencies, we could place all the γ transitions in the ^{30}Mg level scheme. The ^{30}Mg γ rays are listed in Table II. For the γ-ray energy uncertainties, only the statistical errors are shown. The systematic errors are estimated to be 0.2 keV at most. The γ rays labeled with $*$ are the newly observed ones. Those labeled with • are known as due to γ-ray transitions in ^{30}Mg, but

[4]The β-ray energy was measured by the HPGe detector.

TABLE I. Coincidence relations with the 1483-keV γ ray. The symbols ○, △, and × denote that the coincidence relation was confirmed in both the 1483-keV and the listed γ-ray gated spectra, the 1483-keV γ-ray peak was not observed in the listed γ-ray gated spectrum, and the coincidence relation was not confirmed in both the spectra, respectively.

Coincidence	γ ray (keV)						
○	305	956	985	995	1222	1283	1382
	1480	1506	1552	1560	1633	1791	1807
	1821	1898	1952	1978	1980	2060	2158
	2227	2459	2499	2605	2627	2685	2945
	3179	3200	3212	3300	3430	3484	3539
	3598	3625	3930	4415	4583		
△	1152	1871	2618	3612			
×	670	724	797	3542	4297	4967	5022
	5095	5413	5619				

newly observed in the β decay of ^{30}Na. The γ transitions whose placements are revised in the present work, as discussed below, are labeled by ▲.

The evaluated intensities in the Nuclear Data Sheets [1] are also listed in Table II for comparison. In Ref. [1] the γ-ray intensities were evaluated by assuming $I_{\gamma 1483} = 44(3)\%$ and $P_n = 30(4)\%$. Most of the absolute γ-ray intensities in the present work are in good agreement with the adopted intensities [1].

The doublets around 1483 and 1978 keV were assigned as follows: The 1483-keV peak shows a lower energy tail in the 1821-keV γ-ray gated spectrum, as shown in the insets of Fig. 4. Figures 4(a) and 4(b) show the γ-ray coincident spectra gated by the higher- (1482–1486 keV) and lower-energy region (1477–1480 keV) of the ∼1483-keV peak, respectively. Note in the gated spectrum of Fig. 4(b) that the 1483-keV peak appears, and the 1821-keV peak is enhanced, compared with the spectrum of Fig. 4(a), whereas the peaks of 1506 keV and

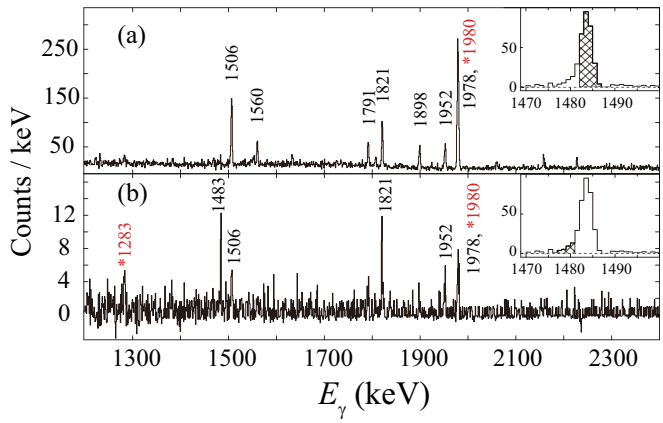

FIG. 4. Gamma-ray coincidence spectra gated by the γ-ray energy regions of (a) 1482–1486 keV and (b) 1477–1480 keV, as shown by the hatched areas in the insets, which show the 1821-keV γ-ray gated spectrum. The peaks labeled with ∗ (shown in red) are newly observed γ rays.

TABLE II. Observed γ rays in ^{30}Mg associated with the β decay of ^{30}Na. The absolute γ-ray intensity I_γ is shown per ^{30}Na decay. The adopted intensities in the Nuclear Data Sheets [1] are also shown. See text for the labels of ∗, •, and ▲.

E_γ (keV)	E_i (MeV)	E_f (MeV)	$I_\gamma^{\rm rel}$	I_γ (%)	
				Present work	Ref. [1]
304.8(1)	1.788	1.483	16.1(12)	6.3(8)	5.1(4)
669.5(3)*	4.967	4.297	0.34(12)	0.13(5)	
724.4(4)*	5.022	4.297	0.215(84)	0.08(3)	
797.4(2)*	5.095	4.297	0.954(86)	0.37(5)	
955.7(1)•	4.259	3.304	1.34(12)	0.52(7)	
984.9(1)	2.468	1.483	14.9(12)	5.8(8)	6.3(5)
994.7(2)*	3.463	2.468	0.413(77)	0.16(3)	
1152.0(3)*	4.695	3.543	1.89(16)	0.7(1)	
1221.9(2)*	4.683	3.461	0.474(94)	0.18(4)	
1283.0(1)*	6.066	4.783	0.95(12)	0.37(6)	
1382.3(1)*	6.066	4.683	0.383(61)	0.15(3)	
1479.5(5)*	4.783	3.304	0.29(17)	0.11(7)	
1483.1(1)	1.483	0	100	39(4)	44(3)
1505.9(1)	4.967	3.461	7.81(63)	3.0(4)	3.7(3)
1552.4(1)	5.095	3.543	3.36(28)	1.3(2)	2.0(2)
1559.6(1)▲	5.022	3.463	2.78(23)	1.1(1)	1.5(2)
1633.2(3)*	5.095	3.461	1.47(13)	0.57(8)	
1791.3(1)	5.095	3.304	3.21(27)	1.3(2)	2.0(3)
1806.6(2)*	6.066	4.259	0.77(11)	0.30(5)	
1820.6(2)	3.304	1.483	5.82(48)	2.3(3)	2.5(2)
1871.0(1)	5.413	3.543	1.24(12)	0.48(7)	0.6(1)
1898.3(1)•	3.381	1.483	2.80(24)	1.1(1)	
1952.0(2)	5.413	3.461	3.28(41)	1.3(2)	2.0(2)
1978.1(1)	3.461	1.483	16.3(23)	6(1)	10.7(9)
1979.6(1)*	3.463	1.483	7.0(10)	2.7(5)	
2059.5(1)	3.543	1.483	0.99(11)	0.39(6)	0.9(1)
2157.6(1)*	5.619	3.461	0.85(32)	0.3(1)	
2226.6(2)*	4.695	2.468	1.10(32)	0.4(1)	
2458.9(3)*	5.922	3.463	0.85(33)	0.3(1)	
2499.3(1)	4.967	2.468	1.61(15)	0.63(9)	0.8(1)
2605.1(2)*	6.066	3.461	1.73(14)	0.68(9)	
2618.0(5)*	5.922	3.304	0.207(58)	0.08(2)	
2627.1(1)	5.095	2.468	1.81(18)	0.7(1)	1.0(1)
2684.5(1)*	6.066	3.381	2.67(24)	1.0(1)	
2945.3(1)*	5.413	2.468	1.20(11)	0.47(6)	
3179.3(1)	4.967	1.788	11.49(95)	4.5(6)	5.3(5)
3200.0(2)*	4.683	1.483	0.98(14)	0.38(7)	
3211.5(2)*	4.695	1.483	2.30(29)	0.9(1)	
3300.1(3)*	4.783	1.483	0.612(83)	0.24(4)	
3430.2(1)*	5.898	2.468	3.74(88)	1.5(4)	
3484.1(1)	4.967	1.483	9.58(80)	3.7(5)	5.1(5)
3539.3(2)	5.022	1.483	1.83(29)	0.7(1)	0.7(3)
3542.4(2)	3.543	0	5.47(55)	2.1(3)	2.9(3)
3597.9(2)*	6.066	2.468	0.899(98)	0.35(5)	
3612.0(3)	5.095	1.483	0.74(33)	0.3(1)	0.4(1)
3625.2(2)	5.413	1.788	2.85(25)	1.1(2)	1.3(2)
3930.2(1)	5.413	1.483	5.59(47)	2.2(3)	2.9(3)
4297.2(3)*	4.297	0	1.34(35)	0.5(1)	
4414.9(1)▲	5.898	1.483	2.49(22)	1.0(1)	1.1(1)
4583.0(1)*	6.066	1.483	0.42(25)	0.2(1)	
4966.8(1)	4.967	0	14.1(12)	5.5(7)	6.8(9)
5022.1(1)	5.022	0	11.43(96)	4.5(6)	5.5(5)
5094.7(1)	5.095	0	6.60(56)	2.6(3)	3.2(3)

TABLE II. (*Continued*.)

E_γ (keV)	E_i (MeV)	E_f (MeV)	$I_\gamma^{\rm rel}$	I_γ (%)	
				Present work	Ref. [1]
5413.0(1)	5.413	0	5.84(50)	2.3(3)	2.8(3)
5618.6(2)*	5.619	0	1.20(13)	0.47(7)	

$\sim$1978 keV are suppressed. These facts suggest that the γ ray in the region of 1477–1480 keV is emitted from a higher level than the 1.483-MeV level, in coincidence with the 1821- and 1483-keV γ rays, but in parallel with the 1506- and $\sim$1978-keV γ rays. The 1483-keV peak was decomposed assuming a doublet, and the peak energies were determined as 1479.5(5) and 1483.1(1) keV. The former energy and the coincidence relations with the 1283- (new), 1821-, and 1483-keV γ rays enabled successful placement of the 1480-keV γ transition as listed in Table II.

The slightly broad peak around 1978 keV was examined by setting energy gates of different γ rays. Figure 5 shows the γ-ray spectra around 1978 keV gated by the 1506- (solid histogram) and 1560-keV (dashed histogram) γ rays. From the gated spectra, the peak energies were determined as 1978.1(1) and 1979.6(1) keV. From the coincidence relations, their transitions were assigned as $4.967 \xrightarrow{\gamma 1506} 3.461 \xrightarrow{\gamma 1978} 1.483$ and $5.022 \xrightarrow{\gamma 1560} 3.463$ (new) $\xrightarrow{\gamma 1980} 1.483$, respectively. Namely, we propose the placement of the 1560-keV γ transition as $5.022 \rightarrow 3.463$, instead of the adopted placement of $5.022 \rightarrow 3.461$ [1].

The 2685- and 3430-keV γ rays were previously reported in Ref. [9], but their placements in the level scheme were missing. As a result, they are not adopted in the γ-ray list [1]. In the present work, new placements for the 2685- and 3430-keV transitions are proposed as 6.066 (new) $\rightarrow$ 3.381 and 5.898 (new) $\rightarrow$ 2.468, respectively. The absolute intensities of the 2685- and 3430-keV γ rays, 1.0(1)% and 1.5(4)%, are consistent with the previously reported intensities of 1.0(4)% and 1.2(4)% [9], respectively.

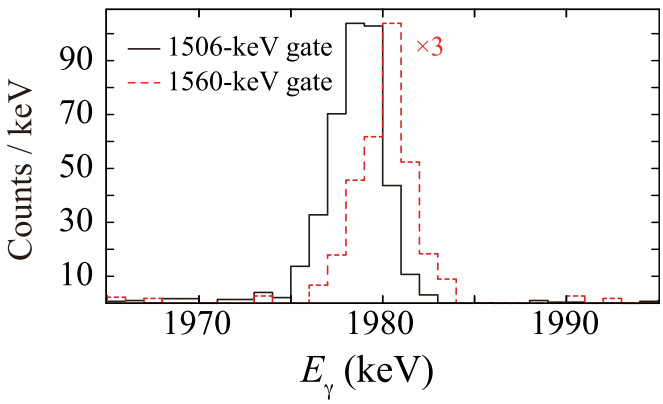

FIG. 5. Gamma-ray coincidence spectra gated by the γ rays of 1506 (solid histogram) and 1560 keV (dashed histogram). The counts of the dashed spectrum are multiplied by 3.

TABLE III. Levels in ^{30}Mg established from the β decay of ^{30}Na. The levels labeled with $*$ are newly proposed in the present work. The levels and transitions labeled with • are known in the reaction data, but observed in the β decay for the first time. The spins and parities labeled with $*$ are newly assigned based on the experimental asymmetry parameter A. The spin and parity assignments labeled with ‡ are proposed from the γ-ray transition relations. The 0^+ assignment for the 1.788-MeV level (labeled with †) was reconfirmed by the present γ-ray angular-correlation measurement.

E_x (MeV)	I^π	A	I_β (%)	log ft	
				Present work	Ref. [1]
0	0^+				
1.4831(1)	2^+		5(1)	6.2(1)	5.86(6)
1.7879(1)	†0^+		0.7(6)	7.0(4)	
2.4680(1)	(2^+)		1.4(6)	6.6(2)	6.12(6)
3.3037(2)	‡(1,2,3)		0.3(2)	7.1(3)	7.0(5)
3.3814(1)•	(4^+)		<0.2	>7.3	
3.4612(2)	‡(2)		<1.3	>6.5	6.01(8)
3.4627(2)*	‡(1,2)		1.5(5)	6.4(2)	
3.5425(1)	‡(2^+)		<0.3	>7.1	6.43(14)
4.2593(3)•	‡(2,3,4)		0.22(6)	7.1(1)	
4.2972(3)*	‡(1,2)		<0.02	>8.1	
4.6831(2)*	‡(2,3,4)		0.42(8)	6.8(1)	
4.6947(2)*	$*3^+$	0.4(3)	2.1(3)	6.1(1)	
4.7831(3)*	‡(2,3,4)		<0.07	>7.5	
4.9670(1)	$*1^+$	−1.01(7)	17(2)	5.1(1)	4.98(4)
5.0222(1)	$*1^+$	−0.94(9)	6.3(8)	5.5(1)	5.42(4)
5.0948(1)	$*2^+$	−0.28(9)	7.1(8)	5.5(1)	5.37(5)
5.4131(1)	$*2^+$	−0.34(8)	7.8(9)	5.4(1)	5.26(5)
5.6187(1)*	$*(1^+, 2^+)$	−0.9(4)	0.8(2)	6.3(1)	
5.8981(1)*	$*1^+$	−0.9(2)	2.4(5)	5.8(1)	
5.9216(2)*			0.4(1)	6.6(1)	
6.0659(1)*	$*3^+$	0.8(2)	3.1(4)	5.6(1)	

The 4415-keV γ ray is listed in Ref. [1] as due to the transition of $4.414 \rightarrow 0$, after Ref. [10]. However, as shown in Table I, the present work confirmed the coincidence relation between the 4415- and 1483-keV γ rays. Therefore, we propose to add a new level at 5.898 MeV and to remove the 4.414-MeV level.

The levels in ^{30}Mg are shown in Table III and in the revised decay scheme of Fig. 6. The ^{30}Mg levels labeled with $*$ are newly proposed in the present work. Note that we have proposed nine new levels in ^{30}Mg.

Table III and Fig. 6 show the absolute β-transition intensities and the log ft values. The fact that $\sum I_\beta + P_n + P_{2n} = 91(8)\%$ indicates that most of the γ rays in $^{30}\text{Na} \rightarrow {}^{30}\text{Mg}$ were observed in the present work, although some of the γ rays might be unobserved. The log ft values in the Nuclear Data Sheets [1] are also shown in Table III for comparison. The log ft values are consistent between the present data and the adopted data. However, because of fragmentation of the β-transition intensity into the new levels, the present log ft values are larger in general than the values in Ref. [1].

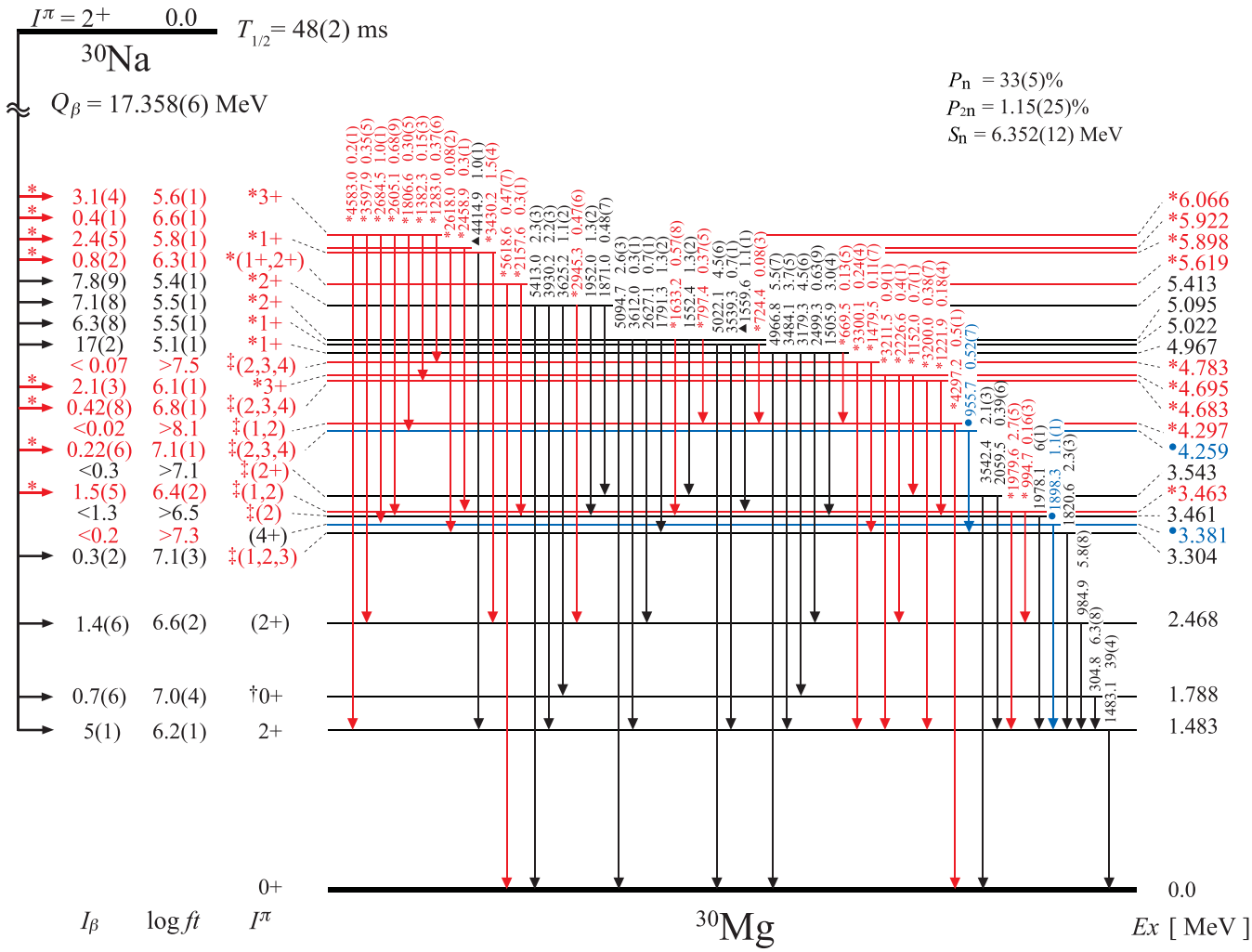

FIG. 6. Revised decay scheme of ^{30}Na $\xrightarrow{\beta}$ ^{30}Mg. The β and γ transitions, levels, and spins and parities labeled with $*$ (displayed in red) are newly established in the present work. The levels and transitions labeled with • (displayed in blue) are known in the reaction data but observed in the β decay for the first time. The γ transitions with revised placements are labeled with ▲. The spin-parity assignments labeled with ‡ are proposed from the γ-ray transition relations. The 0^+ assignment for the 1.788-MeV level (labeled by †) was reconfirmed by the γ-ray angular-correlation measurement.

B. Spin-parity assignments

1. *Reconfirmation of the 0_2^+ assignment for the 1.788-MeV level*

The 0_2^+ assignment for the 1.788-MeV level was proposed because of its long half-life of 3.9(4) ns [1,11]. Later, the 0_2^+ assignment was confirmed by observing the internal-conversion electron in the transition of $0_2^+ \rightarrow 0_1^+$ [12]. Because of the importance of the 0_2^+ assignment, it is desired to reconfirm the assignment in another type of experiment.

We have successfully measured the γ-γ angular correlation between the two cascade γ rays from the 1.788-MeV level: the 305- and 1483-keV γ rays. The present detector setup allowed the correlation angles of 45°, 90°, 135°, and 180°.

Figure 7 shows the results together with the expected angular correlation curves [30] for the possible spin values of the 1.788-MeV level ($I_{1.788} = 0$–4). It is clearly seen that the experimental data are only consistent with the $I_{1.788} = 0$ case.

We have also measured the half-life in the present work to be 3.6(4) ns by the centroid shift method for the time spectra of the β(plastic)-γ_{305}(Ge) (γ_{305}: 1.788 → 1.483) and β-γ_{prompt}. This result is consistent with the adopted half-life and supports the $E2$ nature of the 305-keV transition. Therefore, we reconfirm the 0_2^+ assignment for the 1.788-MeV level.

2. *Spin polarization of ^{30}Na*

The spin polarization of ^{30}Na was determined in a similar way as in the previous work [24]. First, we take notice of two ^{30}Mg levels which are associated with small log ft values and are not populated by γ transitions from higher levels. In the present work the 4.967- [log ft = 5.1(1)] and 5.095-MeV [5.5(1)] levels are picked up. We plausibly assume allowed transitions for these levels, and we apply our method of polarized decay spectroscopy [24].

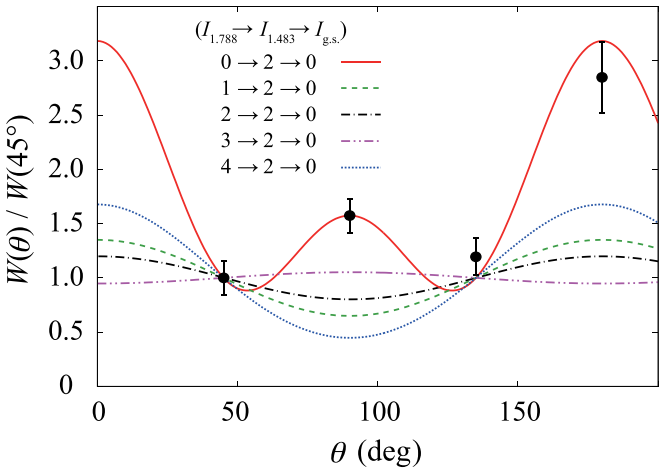

FIG. 7. Angular correlation between the 305-keV [$1.788 \rightarrow 1.483(2_1^+)$] and the 1483-keV [$1.483(2_1^+) \rightarrow 0(0_1^+)$] γ rays. The expected correlation curves are shown for various spin values of the 1.788-MeV level, assuming the lowest multipolarity for each transition.

The number of β-ray counts $N_\theta^\sigma(E_x)$ is necessary to estimate the asymmetry parameter A for β decays leading to the excited level with the excitation energy of E_x. Since θ denotes the position of β detector ($\theta = 0°$ or $180°$) and σ the optical-pumping-laser helicity ($\sigma = +$ or $-$), we have four such numbers of β-ray counts in combinations of θ and σ. Note that, instead of counting the continuous-energy β rays, we count all the deexciting γ rays in coincidence with the β rays. For example, in the case of the β decay to the 4.967-MeV level, the number of β-ray counts, $N_0^+(4.967)$, is obtained by the sum of six γ-ray counts $n_0^+(E_\gamma)$ [$n_\theta^\sigma(E_\gamma)$ for $\theta = 0°$, $\sigma = +$, and the γ-ray energy E_γ, see Table II for the deexciting γ rays]:

$$N_0^+(4.967) = n_0^+(670) + n_0^+(1506) + n_0^+(2499) + n_0^+(3179) + n_0^+(3484) + n_0^+(4967).$$

The numbers of β-ray counts with the other combinations of θ and σ, namely, $N_0^-(4.967)$, $N_{180}^+(4.967)$, and $N_{180}^-(4.967)$, are obtained in the same way. Then, the product $A_{4.967}P$ of the asymmetry parameter $A_{4.967}$ for the β decay of $^{30}\mathrm{Na}_{g.s.} \rightarrow {}^{30}\mathrm{Mg}(4.967)$ and the polarization P is obtained as

$$A_{4.967}P = \frac{\sqrt{R}-1}{\sqrt{R}+1}, \quad R = \frac{N_0^+(4.967)/N_{180}^+(4.967)}{N_0^-(4.967)/N_{180}^-(4.967)}.$$

For the 5.095-MeV level, the number of β-ray counts, $N_\theta^\sigma(5.095)$, is obtained from the γ-ray counts of the 797-, 1552-, 1633-, 1791-, 2627-, 3612-, and 5095-keV peaks.

Since the spin-parity of the ground state of the parent nucleus ^{30}Na is 2^+, the possible spin-parity of the daughter ^{30}Mg states are limited to either 1^+ or 2^+ or 3^+ in the case of an allowed transition. Accordingly, the asymmetry parameter A takes either -1.0 or -0.33 or $+0.67$ [24], respectively, as shown in Table IV.

From the experimental values of $A_{4.967}P = -0.31(1)$ and $A_{5.095}P = -0.085(26)$, the ratio of these values is obtained as $A_{4.967}P/(A_{5.095}P) = A_{4.967}/A_{5.095} = 3.6(10)$. Among nine possible combinations of the spin values $I_{4.967}$ and $I_{5.095}$ of the levels at 4.967 and 5.095 MeV, respectively, the ratio of $A_{4.967}/A_{5.095}$ takes the largest value of 3.0 for the spin combination of $(I_{4.967}, I_{5.095}) = (1, 2)$. The next largest one is 1.0 for the spin combinations of $(I_{4.967}, I_{5.095}) = (1, 1), (2, 2), (3, 3)$. Thus, it is clear that the experimental ratio is only consistent with the case of $(I_{4.967}, I_{5.095}) = (1, 2)$. Namely, the spins and parities of the 4.967- and 5.095-MeV levels are assigned as 1^+ and 2^+, respectively. Consequently, the A values of the β transitions to these levels are determined as $A_{4.967} = -1.0$ and $A_{5.095} = -0.33$ (see Table IV). From the experimental values of $A_{4.967}P$ and $A_{5.095}P$, the polarization is estimated as $P_{4.967} = 0.31(1)$ and $P_{5.095} = 0.26(8)$, respectively. The weighted average results in $P = 0.31(1)$.

TABLE IV. The asymmetry parameter A for the allowed β transition from $^{30}\mathrm{Na}_{g.s.}$ to ^{30}Mg states with spin-parity of I_f^π.

I_i^π ($^{30}\mathrm{Na}_{g.s.}$)	I_f^π (^{30}Mg)	A
2^+	1^+	-1.0
	2^+	-0.33
	3^+	$+0.67$

3. *Spin-parity assignment based on the experimental asymmetry parameter*

We apply the method of polarized decay spectroscopy [24] to the levels at 4.695 [$\log ft = 6.1(1)$], 4.967 [5.1(1)], 5.022 [5.5(1)], 5.095 [5.5(1)], 5.413 [5.4(1)], 5.619 [6.3(1)], 5.898 [5.8(1)], and 6.066 [5.6(1)] MeV, assuming allowed transitions. The parities of these levels are assigned all positive. All these levels are populated solely by β decay, thus it is not necessary to consider the γ feedings from higher levels [24]. The AP value associated with each level is obtained by counting the deexciting γ rays, as was done for the 4.967- and 5.095-MeV levels. Then, the A value is obtained from the experimentally determined P value of 0.31(1). The results are shown in Table III and Fig. 8. Note that the A values for

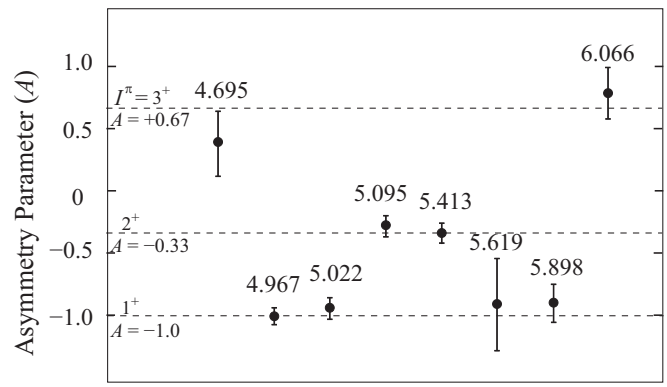

FIG. 8. Experimental asymmetry parameters. The expected values for given spins and parities are shown by the horizontal dashed lines.

the 4.967- and 5.095-MeV levels are reevaluated using the weighted average value of P.

In Fig. 8, the expected A values for the given spin values are shown by the horizontal dashed lines. It is clearly seen that the asymmetry parameters for the 5.022-, 5.413-, 5.898-, and 6.066-MeV levels are very consistent with the spin value of 1, 2, 1, and 3, respectively. Thus, the spins and parities of these levels are firmly assigned as 1^+, 2^+, 1^+, and 3^+, respectively.

The asymmetry parameter for the 4.695-MeV level is consistent with the 3^+ assignment but is barely apart by 2σ from the expected value for the 2^+ assignment. We tentatively assign this level as 3^+. For the 5.619-MeV level the 3^+ assignment is clearly rejected, but it is hard to tell whether 2^+ or 1^+. We assign this level as $(1^+, 2^+)$.

We have tried to evaluate the asymmetry parameters for the lower two levels at 2.468 MeV [$\log ft = 6.6(2)$] and 3.461 MeV [6.6(4)]. However, these levels are populated also by many γ transitions from higher levels, which are associated with different A values. Such a situation causes large errors in A and, as a result, the spin assignments are not possible.

4. Spin-parity assignment based on γ-ray transition relations

Once the spins and parities of the above-mentioned levels are assigned, the γ-ray transition relations suggest spin-parity assignments for other levels, as described below.

Note again the 3.461-MeV level. This level is populated by γ-ray transitions from the 3^+ 6.066-, 2^+ 5.413-, and 1^+ 4.967-MeV levels with comparable intensities, and is depopulated only to the 2_1^+ level. These facts suggest that the adopted (4^+) assignment[5] is not appropriate. We propose to revise the assignment to (2) for the 3.461-MeV level. Either parity is possible.

The known level at 3.304 MeV with no adopted spin-parity assignment is populated from four levels including the 2^+ 5.095-MeV level. The intensities of the $5.095(2^+) \rightarrow 3.304$ and $5.095(2^+) \rightarrow 1.483(2^+)$ transitions are comparable and the latter transition is of $M1$ nature. Thus, the former transition is most likely of $M1$ or $E1$ nature. We propose to assign the 3.304-MeV level as (1,2,3).

The 3.463-MeV level is connected with the 1^+ 5.022-MeV level, which is depopulated by γ-ray transitions to 0_1^+, 2_1^+, and the 3.463-MeV levels with comparable intensities. Since the two former transitions [$5.022(1^+) \rightarrow 0(0_1^+)$, $5.022(1^+) \rightarrow 1.483(2_1^+)$] are of $M1$ nature, the latter transition [$5.022(1^+) \rightarrow 3.463$] is likely of $M1$ or $E1$ nature. Therefore, we propose to assign the spin of the 3.463-MeV level as (1,2).

The adopted spin-parity assignment for the 3.543-MeV level is $(1, 2)^+$ [1]. However, the 1^+ assignment is rejected because the 3.543-MeV level is populated from the 3^+ 4.695-MeV level. Note the fact that this level is depopulated to the 0_1^+ and 2_1^+ levels. Therefore, we propose to assign the spin-parity of the 3.543-MeV level as (2^+).

The 4.259-MeV level is populated from the 3^+ 6.066-MeV level. Therefore, we propose to assign the spin of the 4.259-MeV level as (2,3,4). For the new level at 4.297 MeV, we propose the (1,2) assignment because of the transition of $4.297 \rightarrow 0(0_1^+)$. Similarly, for the new levels at 4.683 and 4.783 MeV, we propose the (2,3,4) assignments because of the transitions to the 2_1^+ level and missing transitions to the 0_1^+ level.

A comment is given here on the recent negative-parity assignment of $(2)^-$ for the 2.468-MeV level [20]. The adopted assignment for this level is (2^+) [1] after Mach *et al.* [11]. It is to be noted that negative-parity levels at such a low-energy region are hardly predicted by any theory to date. Therefore, we follow the (2^+) assignment, and we assume this in the following discussion.

In conclusion, we propose the spin-parity assignments inferred from the γ-ray transition relations as shown by the label ‡ in Table III and Fig. 6.

V. DISCUSSION

A. Level grouping based on experimental information

Since we have established new spin-parity assignments for the levels in ^{30}Mg, it becomes possible to get more insight into nuclear structure of each level than before. Figure 9 shows the experimental levels grouped from the viewpoint of structure, as discussed below. Before comparing the experimental levels with the theoretical calculations, we discuss characteristic features of the levels based solely on the experimental information.

1. Band built on the ground 0_1^+ level

The ^{30}Mg ground-state band up to 4_1^+ was clearly observed by γ-ray spectroscopy for the fusion reaction of ^{14}C(^{18}O, $2p$) [21]. The excitation energy ratio $E(4_1^+)/E(2_1^+) = 2.28$ suggests a vibrational-like structure of this band [31]. This fact

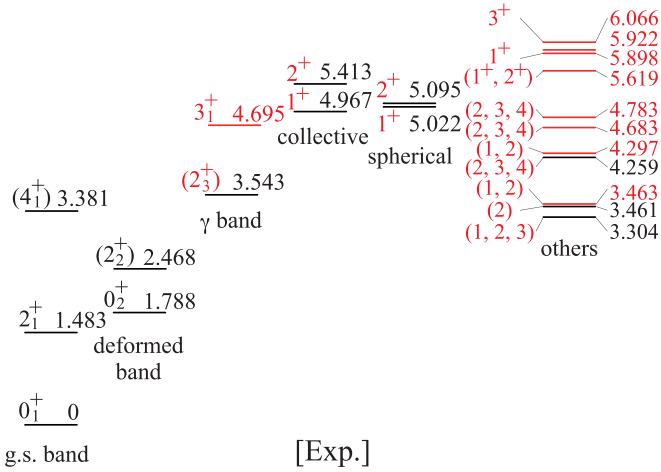

FIG. 9. Experimental levels sorted by structure. New findings in the present work are displayed in red.

[5]From the β-decay data, the $(1, 2, 3)^+$assignment had been adopted for this level, but taking into account the fusion reaction data [21], the evaluated assignment has been changed to (4^+) [1]. However, note that Ref. [21] resolved neither the γ-ray doublet peaks of 1978–1980 keV nor the doublet levels at 3.461 and 3.463 MeV (new level).

requires reconsideration of the naive picture of the spherical 0_1^+ level.

The log ft value for the β decay to ^{30}Mg(2_1^+) is 6.2(1) in the present work. As for the structure of ^{30}Na, it has been shown that the ground state of ^{30}Na exhibits large quadrupole collectivity with the 2p2h intruder configuration [32–35]. Therefore, the somewhat large log ft value is consistent with a major normal configuration of the 2_1^+ level. The log ft value of >7.3 for the 4_1^+ level is consistent with the 4^+ assignment.

2. Band built on the second 0_2^+ level

As discussed before, it was shown that the 0_2^+ level is largely deformed as a result of a significant $\nu f_{7/2}$ intruder configuration. The estimated deformation parameter for the 0_2^+ level was $\beta = 0.59$ [12]. A naive assumption for the 2.468-MeV 2_2^+ level is that it is the rotational 2^+ level of the band built on the 0_2^+ level.

Based on this interpretation, a simple estimation of the 2_2^+ level energy is expressed by using the deformation parameter β as [31]

$$E(2_2^+) = E(0_2^+) + \frac{2(2+1)\hbar^2}{2\mathscr{I}},$$
$$\mathscr{I} = \alpha \mathscr{I}_{\rm rig} = \alpha \frac{2}{5} AMR^2(1 + 0.31\beta),$$

where $\mathscr{I}$, $\mathscr{I}_{\rm rig}$, and α are the moment of inertia of ^{30}Mg nucleus, that of the rigid-body, and the ratio of the two moments of inertia; $\alpha = \mathscr{I}/\mathscr{I}_{\rm rig}$, respectively, and A, M, and R are the mass number, the nucleon mass, and the nuclear radius, respectively. Assuming the experimental value of $\beta = 0.59$ and the empirical value of $\alpha \sim 0.7$ for the ground-state band of ^{24}Mg ($\beta = 0.42$) [36], we obtain $E(2_2^+) \sim 2.69$ MeV, which is in rather good agreement with the experimental energy of 2.468 MeV. Thus, we propose that the 0_2^+ and 2_2^+ levels are the members of the rotational band. The 4^+ member of the deformed band was not assigned in the present work.

3. γ-vibrational band built on the third 2_3^+ level

Note the rather low excitation energy of the third 2_3^+ level at 3.543 MeV. As shown in Table V, this 2_3^+ level is strongly connected with the newly found 3_1^+ level at 4.695 MeV, compared with the other 2^+ levels of 2_1^+ and 2_2^+. In Table V the γ-transition intensities are shown relative to the Weisskopf estimates to take into account the transition energy difference. The strongly connected levels of 2^+ and 3^+ at such a low-excitation-energy region suggest a γ-vibrational band [31]. Therefore, we propose that the 2_3^+ and 3_1^+ levels are members of the γ-vibrational band, as shown in Fig. 9.

TABLE V. Comparison of the experimental γ-ray intensities ($I^{\rm expt}$) of the transitions from the 3_1^+ 4.695-MeV level to the three 2^+ levels. The intensities are shown relative to the Weisskopf estimates ($I^{\rm W.e.}$) assuming $M1$ transitions.

E_i [I^π] (MeV)	E_f [I^π] (MeV)	E_γ (keV)	$I^{\rm expt}/I^{\rm W.e.}$
4.695 [3_1^+]	1.483 [2_1^+]	3212	1
	2.468 [2_2^+]	2227	1.4(5)
	3.543 [2_3^+]	1152	18(3)

A naive picture of the γ-vibrational 2^+ state is a γ-vibrational excitation ($K = 2$) of an axially symmetric 0^+ state. However, an axially asymmetrically deformed component in the 0^+ state causes a lowering of the γ-vibrational 2^+ state [37]. In the present case, it is interpreted that the deformed 0_2^+ level contains some amount of γ-deformed components, and as a result the (quasi-)γ band appears with the bandhead of the 2_3^+ level at 1.76 MeV above the 0_2^+ level.

According to the Davydov model [37], the γ-deformation parameter is estimated from the experimental energies of the deformed 2_2^+ and the γ-vibrational 2_3^+ levels relative to the deformed bandhead 0_2^+ level, namely, $E(2_3^+) - E(0_2^+)$ and $E(2_2^+) - E(0_2^+)$. In the present work, the ratio $[E(2_3^+) - E(0_2^+)]/[E(2_2^+) - E(0_2^+)]$ is estimated to be ∼2.58. This value gives the γ parameter as $\gamma \sim 24^\circ$. Note that even such a large γ value does not significantly affect the energies of the deformed band [31,37] as well as the naive discussion on $E(2_2^+)$ in the previous section.

It should be noted that, in ^{34}Si, which has an N/Z ratio similar to that of ^{30}Mg, it was reported that the 4.519-MeV 2_2^+ level is the bandhead of the γ band with $\gamma \sim 22^\circ$ [38]. The present result suggests a triaxiality of ^{30}Mg similar to that of ^{34}Si.

4. Collective and spherical 1^+ and 2^+ levels around 5 MeV

Next, we focus on the ^{30}Mg levels populated with large β-branching ratios. Note that ∼40% of β-transition intensity goes to four levels around 5 MeV. These are the levels at 4.967 MeV [1^+, $I_\beta = 17(2)\%$, log $ft = 5.1(1)$], 5.413 MeV [2^+, 7.8(9)%, 5.4(1)], 5.095 MeV [2^+, 7.1(8)%, 5.5(1)], and 5.022 MeV [1^+, 6.3(8)%, 5.5(1)]. Interestingly, these levels are selectively deexcited to the lowest four levels, i.e., the 0_1^+, 2_1^+, 0_2^+, and 2_2^+ levels, as shown in Fig. 10.

Since a large β-branching ratio indicates a large overlap of the wave functions between the well-deformed ground state of ^{30}Na [$\beta = 0.41(10)$] [35] and the daughter level, it is suggested that the 1^+ 4.967-MeV level with the largest β-branching ratio is of collective nature. To examine the characteristic features of this level the experimental γ-transition intensities are compared in Table VI. The intensities are shown relative to the Weisskopf estimates.

It is noticed that, as compared with the $4.967[1^+] \rightarrow 0[0_1^+]$ transition, the $4.967[1^+] \rightarrow 1.788[0_2^+]$ transition is three times enhanced, and the $4.967[1^+] \rightarrow 1.483[2_1^+]$ transition is twice enhanced. The intense transition to the deformed 0_2^+ level suggests that the 1^+ 4.967-MeV level is indeed of collective nature. The considerable γ transitions to the 0_1^+ and 2_1^+ states suggest the $npnh$ configuration mixing in these vibrational-like ground-state band members to some extent. It is also reasonable to consider the possibility of the spherical and deformed configuration mixing in the 1^+ 4.967-MeV level itself.

The intense transition to the deformed 0_2^+ level and the energy difference between the 1^+ and 0_2^+ levels (3.179 MeV)

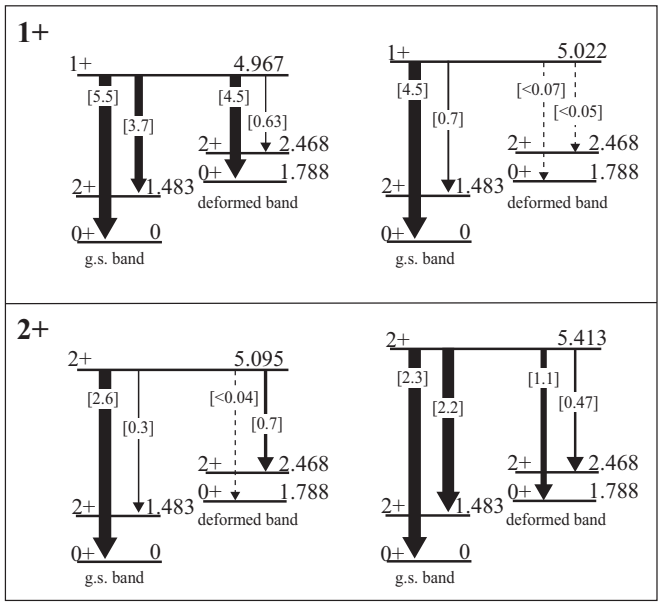

FIG. 10. Experimental γ-ray transitions from the 4.967-MeV 1^+, 5.022-MeV 1^+, 5.095-MeV 2^+, and 5.413-MeV 2^+ levels. The widths of arrows show the γ-ray intensities relative to the most intense one for each initial level. The dotted arrows indicate unobserved transitions. The absolute γ-transition intensities per 100 ^{30}Na decays are shown in square brackets.

remind us of an $M1$ scissors mode. In heavy deformed nuclei, specific $1^+ \sim 3$-MeV levels, which show intense $M1$ transitions to deformed 0^+ and 2^+ states, have been assigned as the $M1$-scissors-mode levels. They are characterized by a vibrational motion of the deformed proton and neutron distributions oscillating with respect to each other, like scissors [31,39]. We tentatively propose that the 1^+ 4.967-MeV level is a candidate for the scissors-mode 1^+ level. Further experimental information, such as $B(M1; 1^+ \rightarrow 0^+)$, and theoretical examination are needed to confirm our proposal.

For the 2^+ 5.413-MeV level, the collective nature is also suggested by the second-largest β-transition intensity and the four-times enhanced γ transition intensity of $5.413[2^+] \rightarrow 1.788[0_2^+]$ as compared with $5.413[2^+] \rightarrow 0[0_1^+]$. The γ transitions to the ground-state band members again suggest the mixed configurations of npnh for the 0_1^+ and 2_1^+ levels, or 0p0h configuration mixing for the 2^+ 5.413-MeV level. The experimental results also suggest 0p0h configuration mixing for the deformed 2_2^+ 2.468-MeV level.

The 1^+ 5.022-MeV and 2^+ 5.095-MeV levels are characterized by weak transitions to the deformed 0_2^+ and 2_2^+ levels, as shown in Fig. 10 and Table VI. This fact suggests spherical nature of the 1^+ 5.022-MeV and 2^+ 5.095-MeV levels. In particular, the unobserved γ transitions from the 1^+ 5.022-MeV level to the deformed band members indicate the major 0p0h configuration of the 1^+ 5.022-MeV level. Contrarily, the considerable intensity of the $5.095[2^+] \rightarrow 2.468[2_2^+]$ transition suggests npnh configuration mixing in the 2^+ 5.095-MeV level.

TABLE VI. Comparison of the experimental γ-transition intensities ($I^{\rm expt}$). The intensity is shown as the ratio to the Weisskopf estimate ($I^{\rm W.e.}$). The assumed multipolarity for the Weisskopf estimate is shown in the last column. The parentheses for the γ-ray energy E_γ indicate that the relevant γ ray was not observed. For such transitions, an upper limit ratio is given, assuming a γ-ray peak with counts of 3σ of the background counts.

E_i [I^π] (MeV)	E_f [I^π] (MeV)	E_γ (keV)	$I^{\rm expt}/I^{\rm W.e.}$	$\sigma\lambda$
4.967 [1^+]	0 [0_1^+]	4967	1	$M1$
	1.483 [2_1^+]	3484	2.0(2)	$M1$
	1.788 [0_2^+]	3179	3.1(4)	$M1$
	2.468 [2_2^+]	2499	0.9(1)	$M1$
5.022 [1^+]	0 [0_1^+]	5022	1	$M1$
	1.483 [2_1^+]	3539	0.46(8)	$M1$
	1.788 [0_2^+]	(3234)	<0.06	$M1$
	2.468 [2_2^+]	(2554)	<0.08	$M1$
5.095 [2^+]	0 [0_1^+]	5095	1	$E2$
	1.788 [0_2^+]	(3307)	<0.13	$E2$
	1.483 [2_1^+]	3612	1	$M1$
	2.468 [2_2^+]	2627	6(3)	$M1$
5.413 [2^+]	0 [0_1^+]	5413	1	$E2$
	1.788 [0_2^+]	3625	3.6(4)	$E2$
	1.483 [2_1^+]	3930	1	$M1$
	2.468 [2_2^+]	2945	0.51(6)	$M1$

5. Other levels

Levels in the very right of Fig. 9, including the 1^+ and 3^+ levels around 6 MeV, are not interpreted only by the experimental information. Further investigations are awaited.

B. Comparison with the CHFB + LQRPA calculation

The experimental data are compared with the theoretical calculation by the CHFB + LQRPA method [18]. This theory has been developed to investigate the large-amplitude collective dynamics by solving the five-dimensional (5D) quadrupole collective Schrödinger equation. The collective masses and potentials of the 5D collective Hamiltonian are microscopically derived with use of the constrained Hartree-Fock-Bogoliubov plus local quasiparticle random-phase approximation (CHFB + LQRPA).

This theory was applied to describe the low-lying collective and spherical states in the even-mass $^{30-36}$Mg nuclei [19]. The CHFB + LQRPA calculation successfully predicts the transition of the spherical and deformed shapes according to the neutron number change.

For ^{30}Mg, the CHFB + LQRPA calculation predicts the ground-state band (0_1^+, 2_1^+, 4_1^+, 6_1^+), the deformed band (0_2^+, 2_2^+, 4_2^+, 6_2^+), and the γ-vibrational band (2_3^+, 3_1^+, 4_3^+, 5_1^+, 6_3^+) [19]. Figures 11(a) and 11(b) show the experimental levels and the predicted levels of ^{30}Mg, respectively. The solid arrows in Fig. 11(a) indicate the experimentally observed γ-ray transitions, and the arrows in Fig. 11(b) are the predicted transitions assuming $E2$ transitions. The dashed arrows in Fig. 11(a) show the theoretically predicted but experimentally unobserved transitions.

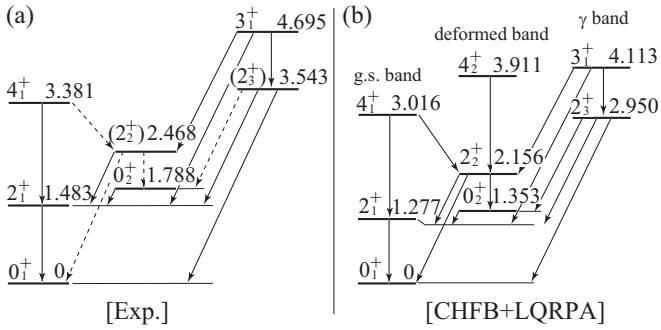

FIG. 11. Three bands in ^{30}Mg of (a) the experimental results and (b) the CHFB + LQRPA calculation [19]. In panel (a) the experimentally observed transitions are shown by the solid arrows, and the unobserved but theoretically predicted transitions by the dashed arrows. In panel (b) the predicted $E2$ transitions are displayed by the solid arrows.

By comparing Figs. 11(a) and 11(b) it is understood that the theoretical prediction supports the experimental level grouping discussed above in Sec. V A. It is found that the level sequence and level energy are reproduced fairly well. Most of the experimental and theoretical γ-transition paths are in good agreement. However, note that three interband transitions of $2_2^+ \to 0_1^+$, $2_3^+ \to 0_2^+$, and $4_1^+ \to 2_2^+$, and the intraband transition of $2_2^+ \to 0_2^+$ are not observed in the present measurement. These facts are likely due to the competition between the $E2$ and $M1$ transitions from each initial level.

For the ground-state band, the probability density plots in the β-γ plane show somewhat spread distributions with peaks around the deformation parameters of $\beta \sim 0.15$ and $\gamma \sim 30^\circ$ [40]. This supports our interpretation of vibrational-like structure. As for the deformed band, almost axially symmetric deformation is predicted at $\beta \sim 0.35$ and $\gamma \sim 15^\circ$. For the γ band built on the 2_3^+ level, a vibrational nature is indeed predicted ($\beta = 0.2$–0.35 and $\gamma = 20^\circ$–30°). The γ parameter is reasonably comparable with the estimated value of $\gamma \sim 24^\circ$ from the Davydov model (see Sec. V A 3). This fact suggests that the mixture of various deformed components in the β-γ plane is not important in ^{30}Mg.

C. Comparison with the AMD + GCM calculation

The present data are also compared with another type of theory, which assumes neither deformation nor a mean field. This theory, named "AMD + GCM theory," is based on the antisymmetrized molecular dynamics (AMD) and the generator coordinate method (GCM) [41]. It successfully explains the deformed ground state of ^{31}Mg [42,43] and predicts shape coexistence of many-particle and many-hole states in a low-excitation-energy region of the neutron-rich $^{31-34}$Mg isotopes [44]. The shape coexistence in ^{31}Mg was experimentally confirmed [23,24].

Figures 12(a) and 12(b) show the experimental ^{30}Mg levels and the ones predicted by the AMD + GCM calculation, respectively. By comparing them, it is seen that the ground-state band and the γ-vibrational band are reasonably reproduced.

However, the deformed band built on the 0_2^+ level is predicted at rather low energy. The lowering seems to be caused by the large mixing with the ground-state band. Negative-parity levels predicted at 2.3–5.0 MeV may correspond to the experimental levels at 3.3–5.6 MeV with large $\log ft$ values.

For the ground-state band, the deformation parameters of $\beta = 0.32$ and $\gamma = 20^\circ$ are predicted. The β value is rather different from that by the CHFB + LQRPA calculation, because, in the AMD + GCM calculation, the γ value is obtained with a fixed β value so as to give the minimum energy. Nevertheless, both theories predict more or less nonspherical nature of the ground-state band. Therefore, the naive picture of spherical ground state has to be revised.

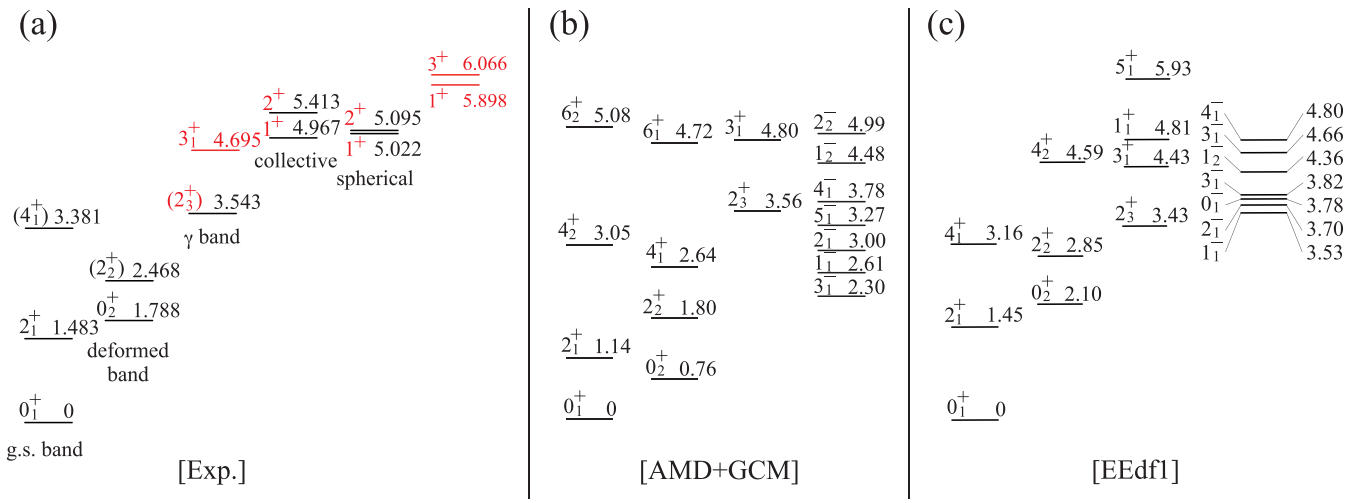

FIG. 12. Comparison between the ^{30}Mg levels (a) established by the present experiment (spin-parity-assigned levels only), (b) predicted by the AMD + GCM calculation, and (c) by the shell-model calculation (EEdf1). In panel (a) the newly assigned levels and spins and parities are displayed in red.

TABLE VII. Probability of npnh configurations in ^{30}Mg levels predicted by the EEdf1 calculation.

I^π	E_x (MeV)	0p0h	2p2h	4p4h	6p6h
0_1^+	0.00	0.244	0.542	0.198	0.016
2_1^+	1.45	0.113	0.629	0.239	0.019
4_1^+	3.16	0.010	0.724	0.249	0.017
0_2^+	2.10	0.254	0.547	0.186	0.013
2_2^+	2.85	0.357	0.501	0.134	0.008
4_2^+	4.59	0.367	0.485	0.139	0.009
2_3^+	3.43	0.221	0.545	0.218	0.016
3_1^+	4.43	0.129	0.599	0.253	0.018
1_1^+	4.81	0.004	0.758	0.226	0.013

D. Comparison with the shell-model calculation

The experimental data are also compared with the large-scale shell-model calculation with the EEdf1 interaction [45]. This interaction is generated by the extended Kuo-Krenciglowa method based on the QCD-based interaction and the three-body force without fitting the two-body matrix elements. The shell-model calculation (hereinafter the "EEdf1 calculation") is performed with the particle-hole configurations up to 6p6h.

Figure 12(c) shows the levels predicted by the EEdf1 calculation. The predicted levels are displayed in four groups: the first group (0_1^+, 2_1^+, 4_1^+), the second group (0_2^+, 2_2^+, 4_2^+), the other positive-parity levels, and negative-parity levels.

By comparing the predicted levels with the experimental ones in Fig. 12(a), it is reasonably assumed that the first and second groups correspond to the experimental ground-state and deformed bands, respectively. The theoretical two levels of the third positive-parity group, i.e., 2_3^+ (3.43 MeV) and 3_1^+ (4.43 MeV), show good correspondence to the experimental γ-band members. These levels show large mixing of 0p0h, 2p2h, and 4p4h configurations, as listed in Table VII. This supports the γ-vibrational band interpretation.

Note that the EEdf1 calculation predicts surprisingly large mixing of the 2p2h configuration for the ground-state band members. This also supports the picture of vibrational-like structure for the ground-state band. As for the deformed band members, although the 2p2h configuration is the largest, the 0p0h configuration prevails to a large extent. The large configuration mixing in the ground-state and deformed bands explains the characteristic properties of the transitions from the levels around 5 MeV, discussed in Sec. V A 4.

The predicted 1^+ level at 4.81 MeV is characterized by the major 2p2h configuration. This fact suggests that this level corresponds to the experimental 1^+ level at 4.967 MeV, which is tentatively proposed as the deformed level with the scissors mode.

VI. SUMMARY

New measurements have been performed for the β decay of spin-polarized ^{30}Na to investigate the structure of ^{30}Mg, which is located in the nuclear chart close to the $N = 20$ "island of inversion" domain.

The high intensity ^{30}Na beam enabled observation of 55 γ-ray peaks in ^{30}Mg (28 more than the adopted). From the detailed γ-γ coincidence relations, nine new states have been established in the level scheme of ^{30}Mg. The highly polarized ^{30}Na beam enabled firm spin-parity assignments of seven states in ^{30}Mg by means of the spatial asymmetry of β-ray counts in coincidence with the ^{30}Mg γ rays. The relations of γ transitions from and to the spin-parity-assigned levels enabled proposals of spin-parity assignments for some other states. Furthermore, the γ-γ angular-correlation measurement enabled reconfirmation of the 0_2^+ assignment in the different type of experiment.

Solely based on the experimental information, it is shown that the various characteristic structures coexist in ^{30}Mg: (i) the ground-state vibrational-like band [0_1^+, 2_1^+, (4_1^+)]; (ii) the deformed band built on the 0_2^+ state [0_2^+, (2_2^+)]; (iii) the γ-vibrational band built on the (2_3^+) state [(2_3^+), 3_1^+]; and (iv) four states around 5 MeV associated with large β-transition probabilities: 1^+ and 2^+ states with spherical nature, and 1^+ and 2^+ states with collective nature. The energy difference between the γ-vibrational 2_3^+ and deformed 0_2^+ states suggests a triaxiality of the γ band similar to that in ^{34}Si. The γ transitions from the four above-mentioned states of (iv) suggest considerable npnh configuration mixing in both the ground-state and the deformed bands. It should be noted that the 1^+ 4.976-MeV state exhibits an $M1$ scissors mode nature.

The ^{30}Mg level structure has been compared with three types of theoretical calculations of the CHFB + LQRPA theory, the AMD + GCM theory, and the large-scale shell model (EEdf1). All these theories reasonably reproduce the three bands. The shell-model calculation shows significant npnh configuration mixing in both the ground-state and deformed bands.

In conclusion, it has been shown that, in ^{30}Mg, the states with various characteristic structures coexist.

ACKNOWLEDGMENTS

The authors are grateful to the TRIUMF staff for their excellent support and the UC_x target development. The authors thank Dr. N. Hinohara for valuable discussions and comments on the CHFB + LQRPA calculation. This work was supported by JSPS KAKENHI Grants of JP25247039, JP15H03659, JP17H02891, JP18K13574, JP18KK0084, and JP19H01926. The present experiment was performed under the program number S1391 at TRIUMF. TRIUMF receives federal funding via a contribution agreement through the National Research Council of Canada.

[1] M. S. Basunia, Nucl. Data Sheets **111**, 2331 (2010); Evaluated Nuclear Structure Data File, National Nuclear Data Center, Brookhaven National Laboratory, http://www.nndc.bnl.gov.

[2] A. G. Artukh, V. V. Avdeichikov, G. F. Gridnev, V. L. Mikheev, V. V. Volkov, and J. Wilczyński, Nucl. Phys. A **176**, 284 (1971).

[3] C. Thibault, R. Klapisch, C. Rigaud, A. M. Poskanzer, R. Prieels, L. Lessard, and W. Reisdorf, Phys. Rev. C **12**, 644 (1975).

[4] C. Détraz, M. Langevin, M. C. Goffri-Kouassi, D. Guillemaud, M. Epherre, G. Audi, C. Thibault, and F. Touchard, Nucl. Phys. A **394**, 378 (1983).

[5] B. H. Wildenthal and W. Chung, Phys. Rev. C **22**, 2260(R) (1980).

[6] E. K. Warburton, J. A. Becker, and B. A. Brown, Phys. Rev. C **41**, 1147 (1990).

[7] K. Blaum, M. J. G. Borge, B. Jonson, and P. Van Duppen, Highlights at ISOLDE, in *60 Years of CERN Experiments and Discoveries* (World Scientific, 2015), pp. 415–436.

[8] C. Détraz, D. Guillemaud, G. Huber, R. Klapisch, M. Langevin, F. Naulin, C. Thibault, L. C. Carraz, and F. Touchard, Phys. Rev. C **19**, 164 (1979).

[9] D. Guillemaud-Mueller, C. Detraz, M. Langevin, F. Naulin, M. De Saint-Simon, C. Thibault, F. Touchard, and M. Epherre, Nucl. Phys. A **426**, 37 (1984).

[10] P. Baumann, Ph. Dessagne, A. Huck, G. Klotz, A. Knipper, Ch. Miehé, M. Ramdane, G. Walter, G. Marguier, H. Gabelmann *et al.*, Phys. Rev. C **39**, 626 (1989).

[11] H. Mach, L. M. Fraile, O. Tengblad, R. Boutami, C. Jollet, W. A. Płóciennik, D. T. Yordanov, M. Stanoiu, M. J. G. Borge, P. A. Butler *et al.*, Eur. Phys. J. A **25**, 105 (2005).

[12] W. Schwerdtfeger, P. G. Thirolf, K. Wimmer, D. Habs, H. Mach, T. R. Rodriguez, V. Bildstein, J. L. Egido, L. M. Fraile, R. Gernhäuser *et al.*, Phys. Rev. Lett. **103**, 012501 (2009).

[13] G. Klotz, P. Baumann, M. Bounajma, A. Huck, A. Knipper, G. Walter, G. Marguier, C. Richard-Serre, A. Poves, and J. Retamosa, Phys. Rev. C **47**, 2502 (1993).

[14] C. M. Mattoon, F. Sarazin, G. Hackman, E. S. Cunningham, R. A. E. Austin, G. C. Ball, R. S. Chakrawarthy, P. Finlay, P. E. Garrett, G. F. Grinyer *et al.*, Phys. Rev. C **75**, 017302 (2007).

[15] B. V. Pritychenko, T. Glasmacher, P. D. Cottle, M. Fauerbach, R. W. Ibbotson, K. W. Kemper, V. Maddalena, A. Navin, R. Ronningen, A. Sakharuk *et al.*, Phys. Lett. B **461**, 322 (1999).

[16] E. Caurier, F. Nowacki, and A. Poves, Nucl. Phys. A **693**, 374 (2001).

[17] T. Otsuka and Y. Tsunoda, J. Phys. G **43**, 024009 (2016).

[18] N. Hinohara, K. Sato, T. Nakatsukasa, M. Matsuo, and K. Matsuyanagi, Phys. Rev. C **82**, 064313 (2010).

[19] N. Hinohara, K. Sato, K. Yoshida, T. Nakatsukasa, M. Matsuo, and K. Matsuyanagi, Phys. Rev. C **84**, 061302(R) (2011); *International Conference on Advances in Radioactive Isotope Science - ARIS 2011, Leuven, Belgium, 2011*, https://www.hyperfine2016.be/event/0/contributions/354/.

[20] B. Fernández-Domínguez, B. Pietras, W. N. Catford, N. A. Orr, M. Petri, M. Chartier, S. Paschalis, N. Patterson, J. S. Thomas, M. Caamaño *et al.*, Phys. Lett. B **779**, 124 (2018).

[21] A. N. Deacon, J. F. Smith, S. J. Freeman, R. V. F. Janssens, M. P. Carpenter, B. Hadinia, C. R. Hoffman, B. P. Kay, T. Lauritsen, C. J. Lister *et al.*, Phys. Rev. C **82**, 034305 (2010).

[22] M. Wang, G. Audi, F. G. Kondev, W. J. Huang, S. Naimi, and X. Xu, Chin. Phys. C **41**, 030003 (2017).

[23] H. Nishibata, T. Shimoda, A. Odahara, S. Morimoto, S. Kanaya, A. Yagi, H. Kanaoka, M. R. Pearson, C. D. P. Levy, and M. Kimura, Phys. Lett. B **767**, 81 (2017).

[24] H. Nishibata, S. Kanaya, T. Shimoda, A. Odahara, S. Morimoto, A. Yagi, H. Kanaoka, M. R. Pearson, C. D. P. Levy, M. Kimura, N. Tsunoda, and T. Otsuka, Phys. Rev. C **99**, 024322 (2019).

[25] O. Niedermaier, H. Scheit, V. Bildstein, H. Boie, J. Fitting, R. von Hahn, F. Köck, M. Lauer, U. K. Pal, and H. Podlech *et al.*, Phys. Rev. Lett. **94**, 172501 (2005).

[26] J. Dilling and R. Krücken, Hyperfine Interact. **225**, 111 (2014).

[27] C. D. P. Levy, M. R. Pearson, R. F. Kiefl, E. Mané, G. D. Morris, and A. Voss, Hyperfine Interact. **225**, 165 (2014).

[28] T. Shimoda, K. Tajiri, K. Kura, A. Odahara, M. Suga, Y. Hirayama, N. Imai, H. Miyatake, M. Pearson, C. D. P. Levy *et al.*, Hyperfine Interact. **225**, 183 (2014).

[29] T. A. Hinners, V. Tripathi, S. L. Tabor, A. Volya, P. C. Bender, C. R. Hoffman, S. Lee, M. Perry, P. F. Mantica, A. D. Davies *et al.*, Phys. Rev. C **77**, 034305 (2008).

[30] L. C. Biedenharn and M. E. Rose, Rev. Mod. Phys. **25**, 729 (1953).

[31] R. F. Casten, in *Nuclear Structure from a Simple Perspective*, edited by P. E. Hodgson (Oxford University Press, New York, 1990).

[32] G. Huber, F. Touchard, S. Büttgenbach, C. Thibault, R. Klapisch, H. T. Duong, S. Liberman, J. Pinard, J. L. Vialle, P. Juncar, P. Jacquinot *et al.*, Phys. Rev. C **18**, 2342 (1978).

[33] M. Seidlitz, P. Reiter, R. Altenkirch, B. Bastin, C. Bauer, A. Blazhev, N. Bree, B. Bruyneel, P. A. Butler, J. Cederkäll *et al.*, Phys. Rev. C **89**, 024309 (2014).

[34] M. Petri, P. Fallon, A. O. Macchiavelli, S. Heil, E. Rodriguez-Vieitez, D. Bazin, C. M. Campbell, R. M. Clark, M. Cromaz, A. Gade *et al.*, Phys. Lett. B **748**, 173 (2015).

[35] B. V. Pritychenko, T. Glasmacher, P. D. Cottle, R. W. Ibbotson, K. W. Kemper, K. L. Miller, L. A. Riley, and H. Scheit, Phys. Rev. C **66**, 024325 (2002).

[36] A. Bohr and B. R. Mottelson, *Nuclear Structure* (Benjamin, New York, 1975), Vol. II.

[37] A. S. Davydov and G. F. Filippov, Nucl. Phys. **8**, 237 (1958).

[38] R. Han, X. Q. Li, W. G. Jiang, Z. H. Li, H. Hua, S. Q. Zhang, C. X. Yuan, D. X. Jiang, Y. L. Ye, J. Li *et al.*, Phys. Lett. B **772**, 529 (2017).

[39] K. Heyde, P. von Neumann-Cosel, and A. Richter, Rev. Mod. Phys. **82**, 2365 (2010).

[40] N. Hinohara, 2020 (private communication).

[41] M. Kimura, Phys. Rev. C **69**, 044319 (2004).

[42] G. Neyens, M. Kowalska, D. Yordanov, K. Blaum, P. Himpe, P. Lievens, S. Mallion, R. Neugart, N. Vermeulen, Y. Utsuno, and T. Otsuka, Phys. Rev. Lett. **94**, 022501 (2005).

[43] M. Kimura, Phys. Rev. C **75**, 041302(R) (2007).

[44] M. Kimura, Int. J. Mod. Phys. E **20**, 893 (2011).

[45] N. Tsunoda, T. Otsuka, N. Shimizu, M. Hjorth-Jensen, K. Takayanagi, and T. Suzuki, Phys. Rev. C **95**, 021304(R) (2017).